Research papers

Sensitivity of potential evapotranspiration to meteorological factors and their elevational gradients in the Qilian Mountains, northwestern China

Yong Yang*, Rensheng Chen*, Yaoxuan Song, Chuntan Han, Junfeng Liu, Zhangwen Liu

Qilian Alpine Ecology and Hydrology Research Station, Key Laboratory of Ecohydrology of Inland River Basin, Northwest Institute of Eco-Environment and Resources, Chinese Academy of Sciences, Lanzhou 730000, China

ARTICLE INFO

ABSTRACT

Mountainous regions are important sources of freshwater. Measurement of actual evapotranspiration (ET) is difficult to obtain in high mountain regions because of the harsh natural environment, and potential ET (PET) is therefore a suitable term to describe the atmospheric water demand of land surfaces under given meteorological conditions in those high elevation areas. In situ measured meteorological data were collected in 2015 and 2016 from five meteorological stations at various elevations from 2980 m to 4484 m in the Qilian Mountains, northwestern China, and the meteorological factors changed markedly with elevation. PET calculated with the Penman method showed a significant elevational gradient, and decreased as the elevation increased. The sensitivity analysis indicated that over the whole period, PET in the research region was most sensitive to net radiation (RN), followed by relative humidity (RH), air temperature (T), wind speed (WS) and soil heat flux (G). When RN was positive, the sensitivity of PET to RN decreased as the elevation increased, and when RN was negative, the sensitivity increased as the elevation increased. When T was above 0 °C, the sensitivity of PET to T decreased as the elevation increased, and when T was below 0 °C, the sensitivity increased as the elevation increased. The higher the elevation, the greater the sensitivity of PET to both RH and WS. The topographic shading in mountainous regions affected meteorological factors, PET and its sensitivity to meteorological factors in those high elevation areas. The RN was relatively small at the sites with topographic shading because of the reduction in solar radiation, and resulted in less sensitivity of PET to RN and greater sensitivity of PET to other meteorological factors. This study can help us to understand PET in the Qilian mountains and in other mountain regions from which meteorological data are difficult to obtain and very sensitive to climate change.

1. Introduction

Mountain catchments are key sources for river water and water supplies (Dettinger, 2014); 7% of the global mountain area plays an essential role in water resources, whilst another 37% provides important supportive supply, especially in arid and semiarid regions that are vulnerable to seasonal and regional water shortages (Viviroli et al., 2007, 2011). As climates change, sensitive high mountain cold regions can act as reliable indicators of the responses to global warming (Beniston and Stoffel, 2014; Mountain Research Initiative EDW Working Group, 2015; Rogora et al., 2018). Mountain catchments have shown warnings of change in land surface hydrology (Milano et al., 2015), and the hydrological balance and possible future changes in mountainous regions remain poorly understood (Ragettlia et al., 2016). Evapotranspiration (ET), along with precipitation and runoff, is a major component of the water cycle at or near land surfaces in large regions (Senay et al., 2011; Yin et al., 2013), and is thus considered to be the most appropriate indicator of the activity of climate change and water cycle (Wang et al., 2013). Because ET shows great variability over time and space, it is perhaps the most difficult and complicated component in the hydrological cycle (Li et al., 2014). The complex terrain in mountainous regions and the scarcity of measurement data because of the harsh natural environmental conditions exacerbate the lack of understanding of ET in mountainous regions.

The actual ET is the best parameter for characterising the hydrological cycle, but measurement of the actual ET in high mountain regions presents many challenges and difficulties (Yang et al., 2017a). The biggest challenge is that the low temperatures in these cold high-mountain regions test the endurance of field workers and their instruments (Woo, 2008). Since the actual ET is difficult to measure directly,

as an alternative, it can be calculated using mathematical models, usually relying on reference ET or potential ET (PET) (Allen, 2006; Almorox et al., 2015). The reference ET is taken from a reference surface, which is a hypothetical grass reference crop with specific characteristics (Allen et al., 1998). PET refers to the maximum moisture loss from the surface, as determined by the meteorological conditions and the surface type, assuming an unlimited moisture supply (Lhomme, 1997). PET provides the upper limit of land surface ET, while the estimation of actual ET in hydrological models is generally based on PET and crop coefficient (Allen, 2006; Douglas et al., 2009), becomes the common and important input for hydrological models (Li et al., 2016; Wang et al., 2017). As the indicator of evaporative power of atmosphere, PET determines the maximum possible water consumption from the land surface (Wang et al., 2017), therefore become the most suitable term to describe the atmospheric water demand of land surfaces under given meteorological conditions (Zheng et al., 2017).

PET is an integrated measure of four key meteorological variables, including radiation, wind speed, temperature and vapor pressure (Donohue et al., 2010; Sun et al., 2016), and the dominant factors that affect PET show regional differences. In the Yangtze River Basin in China, the decline in PET during the past several decades was attributed to a decrease solar radiation (Wang et al., 2007), whilst wind speed was the dominant factor in the Canadian Prairies (Burn and Hesch, 2007) and Australia (Roderick et al., 2007; McVicar et al., 2012). Furthermore, water vapor and temperature were found to be the dominant factors in a few regions (e.g. Tabari et al., 2012; Zhang et al., 2013). Most studies of PET were based on measurements from national meteorological stations and discussed PET trends in time series and their sensitivity to meteorological parameters (e.g. Zuo et al., 2012; Li et al., 2015, 2017; Peng et al., 2017; Robinson et al., 2017). National meteorological stations are generally located far from each other, and the interpolated gridded datasets from those stations across various climate zones may not provide spatially explicit PET data at high mountainous regions. The complex terrain in high mountain regions may affect the distribution of meteorological elements and thereby affect the spatial distribution of PET. Climatic conditions change markedly with elevation, and PET depends greatly upon elevation (van den Bergh et al., 2013). PET is affected by variations in meteorological factors, but the relationships among these factors and elevation remain unclear (Wang et al., 2016). Therefore, the calculation of PET from datasets based on in situ measurement in a small catchment with the same climatic zone may improve our understanding of ET and its elevational gradient in mountainous regions.

The Qilian Mountains, located at the northeastern edge of the Tibetan Plateau, are the runoff formation zone and the source of all rivers in the arid Hexi Corridor region (Feng, 2010; Dong et al., 2015), which was the main path of the ancient Silk Road and the most important communication route between western and eastern Eurasia (Zhou et al., 2016). Therefore, research into PET and its sensitivity to meteorological factors is of vital significance to understand the water cycle in the Qilian Mountains and water resource management in the oasis belt at the piedmont plain in the Hexi Corridor.

The objectives of this study are: (1) to calculate PET at five elevation sites, (2) to assess the sensitivity of PET to meteorological factors; and (3) to estimate the elevational gradients of sensitivity of PET to meteorological factors in the Qilian Mountains.

2. Data and methods

2.1. Study area and data collection

The Hulu catchment, located in the Qilian Mountains, northwestern China, ranges from 99°49′ E to 99°54′E longitude and from 38°12′N to 38°17′N latitude, with an altitude range from 2960 m to 4800 m and a drainage area of 23.1 km^2 (Fig. 1). A cryosphere-hydrology observation system was established in this small alpine catchment in 2008 (Chen et al.,

2014). In 2008, four automatic meteorological stations were positioned at various elevations. The underlying surfaces were covered by grassland (99°52.9′E, 38°16.1′N, 2980 m), shrub meadow (99°52.6′E, 38°14.9′N, 3232 m), swamp meadow (99°53.4′E, 38°13.9′N, 3711 m) and moraine (99°53.4′E, 38°13.3′N, 4164 m) (Fig. 1). Meteorological factors were measured at each station, included four-component radiation (downward and upward shortwave radiation, downward and upward longwave radiation), air temperature (T), relative humidity (RH), wind speed (WS) and direction, multiple layers of soil moisture and temperature, land surface temperature, soil heat flux (G), precipitation, snow depth. In June 2014, an automatic meteorological station was installed near the Shiyi glacier in the Hulu catchment (Fig. 1), and the underlying surface was covered by moraine (99°52.6′E, 38°13.1′N, 4484 m). Unlike the first four automatic meteorological stations, this station near the Shiyi glacier, did not gather complete meteorological data, only four-component radiation, T, RH, WS, wind direction and precipitation.

The net radiation (RN), is the difference between incoming and outgoing radiation of both short and long wavelengths, and RN is calculated as followed:

$$R_n = R_{s\downarrow} + R_{l\downarrow} - R_{s\uparrow} - R_{l\uparrow} \tag{1}$$

where $R_{s\downarrow}$, $R_{l\downarrow}$, $R_{s\uparrow}$ and $R_{l\uparrow}$ is downward shortwave radiation (MJ·m^{-2}·day^{-1}), downward longwave radiation (MJ·m^{-2}·day^{-1}), upward shortwave radiation (MJ·m^{-2}·day^{-1}) and upward longwave radiation (MJ·m^{-2}·day^{-1}), respectively. The positive of RN means downward radiation, and the negative means upward radiation. The positive of G means upward radiation, and the negative means downward radiation. The meteorological data in this study were gathered from those five meteorological stations, which in this study are named SN2980, SN3232, SN3711, SN4164 and SN4484 in this study (Fig. 1 and Table 1). To compare meteorological factors and PET over the same period, 2 years (2015 and 2016) were selected as the research period.

2.2. Methods

2.2.1. Penman method

A multitude of methods are used to calculate PET (Xu and Singh, 2002; Li et al., 2016), and the Penman method performs reasonably across the range of conditions tested (e.g. Donohue et al., 2010; Milly and Dunne, 2016; Zheng et al., 2017). The land-cover and plant types were different at five research site. In order to reduce the influences from land surface conditions, the Penman method based on the assumption of water surface was chosen to compare the PET and its sensitivity to meteorological factors at different research sites. The Penman method for calculating PET can be expressed as:

$$PET = \frac{\Delta(R_n - G) + 6.43\gamma(1 + 0.536u_2)(e_s - e_a)}{(\Delta + \gamma)\lambda} \tag{2}$$

where PET is the potential ET (mm·day^{-1}); R_n is the net radiation at the surface (MJ·m^{-2}·day^{-1}); G is the soil heat flux (MJ·m^{-2}·day^{-1}); u_2 is the wind speed at a height of 2 m (m·s^{-1}); e_s is the saturation vapor pressure at daily mean air temperature (T_a) (kPa); e_a is the actual vapor pressure (kPa); Δ is the slope of the saturated water vapor pressure curve (kPa·°C^{-1}); and λ is the latent heat of evaporation (MJ·kg^{-1}):

$$\lambda = 2.501 - 0.002361 \times T_a \tag{3}$$

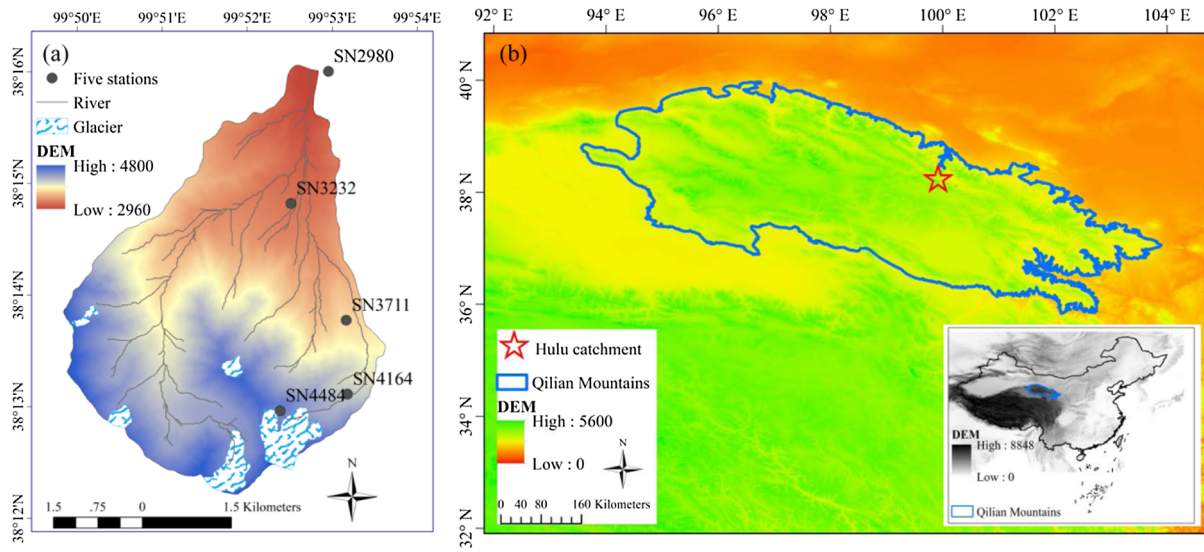where T_a is the average air temperature at a height of 2 m (°C); γ is the psychrometric constant (kPa·°C^{-1}):

$$\gamma = C_P P/(\varepsilon\lambda) \tag{4}$$

where C_p is the specific heat at a constant pressure (1.013 $\times 10^{-3}$ MJ·kg^{-1}·°C^{-1}); ε is the ratio of the molecular weight of water vapor to that for dry air (0.622); and P is atmospheric pressure:

$$P = 101.3 \times ((293 - 0.0065z)/293)^{5.26} \tag{5}$$

where z is the elevation above sea level (m).

Fig. 1. Location of the five automatic meteorological stations in the Hulu catchment (a) and the location of the Hulu catchment in the Qilian Mountains, northwestern China (b).

2.2.2. Sensitivity analysis

The sensitivity coefficient in this study indicates the sensitivity of PET to the meteorological variable, and it is favored to quantify the determining factors in PET. To be dimensionless, the relative sensitivity coefficient (S) is calculated by the partial derivative (McCuen, 1974):

$$S_{v_i} = \lim_{v_i \to 0} \left(\frac{\Delta PET/PET}{\Delta v_i/v_i} \right) = \frac{\partial PET}{\partial v_i} \cdot \frac{v_i}{PET} \tag{6}$$

where S_{v_i} is the sensitivity coefficient of meteorological factor v_i, ΔPET is the variation in PET, v_i is the meteorological factor and Δv_i is the variation of the meteorological factor. A positive/negative S_{v_i} indicates that the PET will increase/decrease as the meteorological factor increases. The greater the S_{v_i}, the greater the effects of the meteorological factor on PET. The analytical expressions can be found in the supplementary material. The sensitivity coefficient has been widely used in ET studies (e.g. Yin et al., 2010; Liu et al., 2012; Zuo et al., 2012; Li et al., 2015; Paparrizos et al., 2016; Li et al., 2017). In this study, RN, G, T, RH and WS were chosen to analyse the sensitivity of meteorological factors to PET, and their sensitivity coefficients were labelled Srn, Sg, St, Srh and Su, respectively.

The daily variations in the meteorological factors in mountainous areas are greatly influenced by local terrain, clouds and fog, and it is difficult to establish a daily-scale elevational gradient. In this study, the meteorological factors and their sensitivity coefficients on PET were analysed on monthly scales by using monthly meteorological quantities, and the seasonal and yearly sensitivity coefficients were obtained by averaging monthly values.

2.2.3. Soil heat flux for SN4484 site

The data for G were measured at the SN2980, SN3232, SN3711 and SN4164 sites, but not at the SN4484 site. Allen et al. (1998) recommended two simple ways to calculate G for monthly period:

$$G_{m,i} = 0.07(T_{m,i+1} - T_{m,i-1}) \tag{7}$$

$$G_{m,i} = 0.14(T_{m,i} - T_{m,i-1}) \tag{8}$$

where $G_{m,i}$ is the soil heat flux density of month i (MJ·m^{-2}·day^{-1}); $T_{m,i}$, $T_{m,i-1}$ and $T_{m,i+1}$ are the mean air temperatures of month i, the previous month and the next month (°C).

In consideration of the form of Eqs. (7)–(8), the following regression formula was built:

$$G_{m,i} = aR_{ms,i} + bR_{ns,i} + c(T_{m,i+1} - T_{m,i-1}) + d(T_{m,i} - T_{m,i-1}) \tag{9}$$

where $R_{ms,i}$ and $R_{ns,i}$ is the solar radiation and the RN of month i (MJ·m^{-2}·day^{-1}), respectively; a, b, c and d are taken from regression analysis with data from the SN4164 site, with a similar underlying surface as the SN4484 site, and with values of -0.0493, 0.1485, 0.0431 and 0.0375, respectively. Fig. 2 showed that the comparison of calculation by Eqs. (7)–(9) and the measured G at the SN4164 site, and their relationship showed that Eq. (9) could more effectively calculate G than Eq. (7) or (8) at the SN4164 site. SN4484 site has an underlying land cover similar to that of the SN4164 site, so it is reasonable to calculate G with Eq. (9) at the SN4484 site.

3. Results

3.1. Elevational gradients of meteorological factors

3.1.1. Net radiation

The mean annual RN measurements at the SN2980, SN3232, SN3711, SN4164 and SN4484 sites in 2015 and 2016 were 7.85 MJ·m^{-2}·day^{-1},

Table 1

In situ field location, land-cover type and observation items of five automatic meteorological stations in the Hulu catchment.

Station name	Longitude (°)	Latitude (°)	Elevation (m)	Land-cover	Data gathered[*]
SN2980	99.883	38.269	2980	Grassland	4R, T, RH, WS, WD, SWC, ST, G, P, SD
SN3232	99.877	38.249	3232	Shrub meadow	4R, T, RH, WS, WD, SWC, ST, G, P, SD
SN3711	99.889	38.232	3711	Swamp meadow	4R, T, RH, WS, WD, SWC, ST, G, P, SD
SN4164	99.890	38.221	4164	Moraine	4R, T, RH, WS, WD, SWC, ST, G, P, SD
SN4484	99.877	38.218	4484	Moraine	4R, T, RH, WS, P

* 4R, four-component radiation (downward and upward shortwave radiation, downward and upward longwave radiation). T, air temperature. RH, relative humidity. WS, wind speed. WD, wind direction. SWC, soil water content. ST, soil temperature. G, soil heat flux. P, precipitation. SD, snow depth.
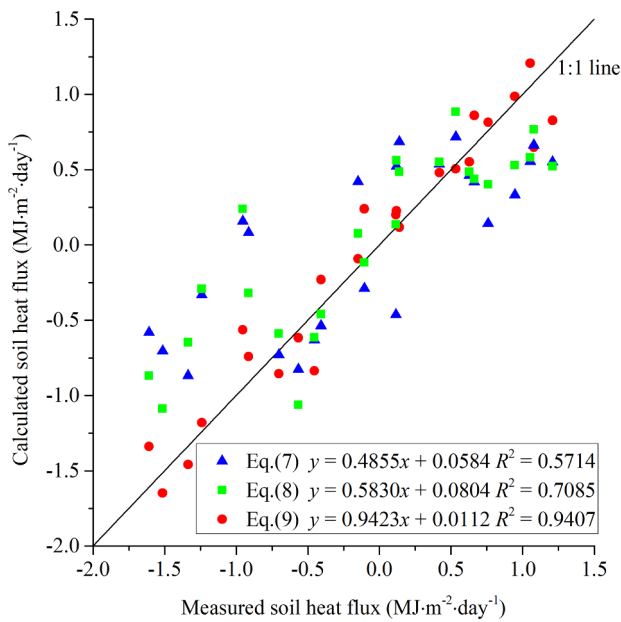
Fig. 2. Comparison of calculations by Eqs. (7)–(9) and the measured soil heat flux at the SN4164 site.

6.74 MJ·m^{-2}·day^{-1}, 4.34 MJ·m^{-2}·day^{-1}, 4.36 MJ·m^{-2}·day^{-1} and 4.63 MJ·m^{-2}·day^{-1}, respectively. The RN showed significant seasonal variation at all five research sites (Fig. 3a). At the beginning of the year, the RN was low, and then it increased until reaching its maximum in July. In autumn, the RN began to decrease because the decrease of solar radiation and the increase of albedo from snow cover caused the decrease of net shortwave radiation. The RN reached its minimum in December and began to increase the next year, entering another cycle. Topographic shading from surrounding terrain was seen at the SN3711 and SN4164 sites in the cold season, which could not be ignored, and the topographic shading at those two sites lasted from October to next March. Thus, the research period in this study was divided into a warm season (April, May, June, July, August and September) and a cold season (January, February, March, October, November and December).

According to the measured data from the five automatic meteorological stations, the RN showed a significant linear elevational gradient relationship during the warm season, and the mean RN decreased about 0.242 MJ·m^{-2}·day^{-1} for each 100 m of 100 m (Fig. 3b, correlation coefficient $R^2 = 0.97$). The annual elevational gradient of the RN over the whole research period (2 years) was about -0.224 MJ·m^{-2}·day^{-1}·100 m^{-1} ($R^2 = 0.75$), but it was not as significant as that during the warm season because the measured RN in the cold season from five stations showed a weak elevational gradient ($R^2 = 0.41$). The mean monthly RN measurements in the cold season at the SN3711 and SN4164 sites were significantly lower than those from the other three researcher sites (Fig. 3b) because of topographic shading in the cold season. Thus, the elevational gradient for the RN in the cold season or over the whole period was more reasonable when the results were calculated from the three meteorological stations that did not have topographic shading. Under this circumstance, the RN elevational gradient was about -0.200 MJ·m^{-2}·day^{-1}·100 m^{-1} for the whole period and -0.147 MJ·m^{-2}·day^{-1}·100 m^{-1} for the cold season.

3.1.2. Soil heat flux

The mean annual G at SN2980, SN3232, SN3711, SN4164 and SN4484 sites in 2015 and 2016 were 0.09 MJ·m^{-2}·day^{-1}, -0.25 MJ·m^{-2}·day^{-1}, 0.03 MJ·m^{-2}·day^{-1}, -0.10 MJ·m^{-2}·day^{-1} and -0.13 MJ·m^{-2}·day^{-1}, respectively. G showed significant seasonal variation at all five research sites (Fig. 4a). At the beginning of the year, the G was negative (upward heat conduction towards relatively cold air); it then increased and became positive in March and reached its
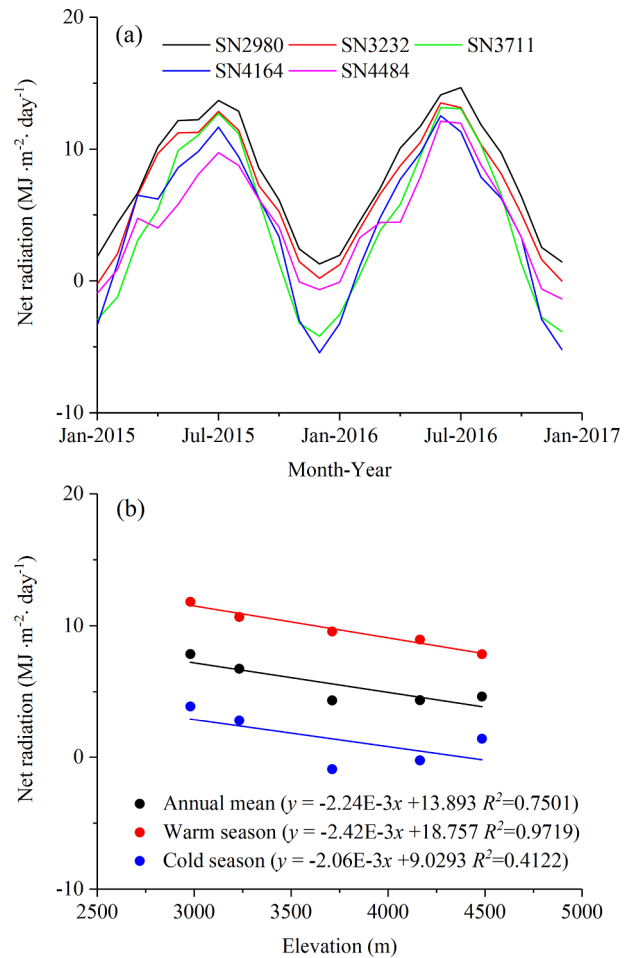

Fig. 3. Variations in the monthly net radiation (a) and the relationship between net radiation and elevation (b) in the Hulu catchment.

maximum in summer. G decreased in autumn, became negative in September, reached its minimum in December and began to increase the next year, entering another cycle. G is relatively low and may be ignored for day time steps, and it is related to RN, its mineral composition and its water content (Allen et al., 1998). The elevational gradient of G during the warm season in the Hulu catchment was -0.0188 MJ·m^{-2}·day^{-1}·100 m^{-1} ($R^2 = 0.93$) (Fig. 4b). However, no significant linear elevational gradients were seen for the cold season or for the whole period (Fig. 4b).

3.1.3. Air temperature

The mean T at the SN2980, SN3232, SN3711, SN4164 and SN4484 sites in 2015 and 2016 was 1.05 °C, -0.78 °C, -1.50 °C, -3.76 °C, and -6.19 °C, respectively. T showed significant seasonal variations at all five research sites. The maximum T usually occurred in July or August, whilst the minimum generally occurred in January (Fig. 5a). It is well known that the elevational gradient of T varies from about -0.98 °C·100 m^{-1} for dry air to about -0.40 °C·100 m^{-1} for very warm saturated air and that the mean lapse rate is -0.65 °C·100 m^{-1} (Dodson and Marks, 1997). According to the data measured from the five automatic meteorological stations, mean T showed a significant linear elevational gradient relationship in the warm season, the cold season and during the whole period with elevational gradients in the research region was -0.54 °C·100 m^{-1} ($R^2 = 0.97$), -0.34 °C·100 m^{-1} ($R^2 = 0.92$) and -0.44 °C·100 m^{-1} ($R^2 = 0.95$), respectively (Fig. 5b).

3.1.4. Relative humidity

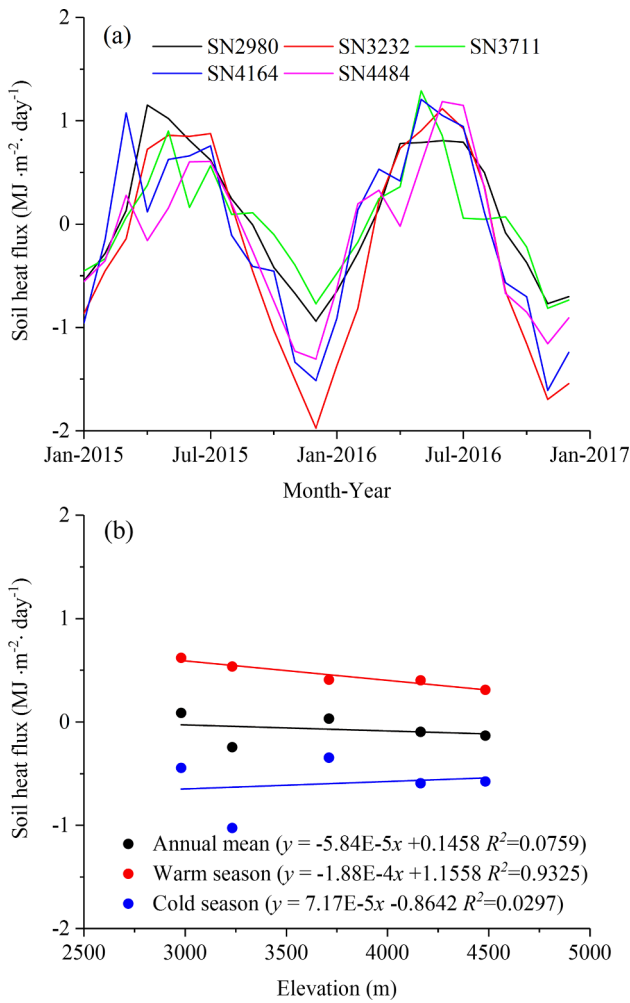The mean RH at the SN2980, SN3232, SN3711, SN4164 and SN4484

Fig. 4. Variations in the monthly soil heat flux (a) and the relationship between soil heat flux and elevation (b) in the Hulu catchment.
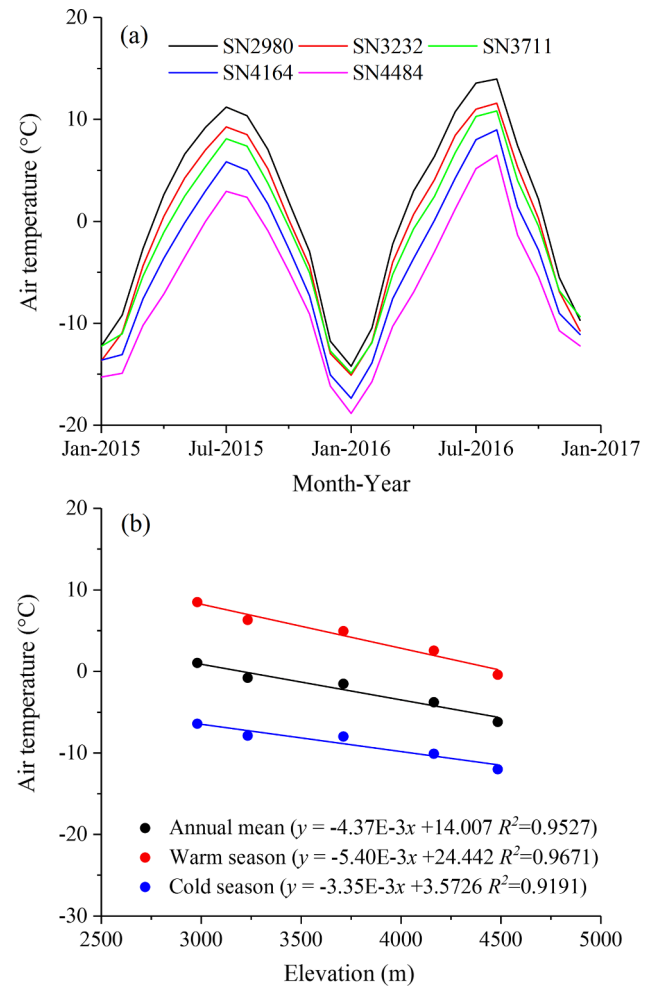

Fig. 5. Variations in the monthly air temperature (a) and the relationship between air temperature and elevation (b) in the Hulu catchment.

sites in 2015 and 2016 were 56.00%, 53.34%, 55.31%, 52.84%, and 55.57%, respectively. Like RN, G and T, RH showed significant seasonal variation at all five research sites; it was low in the cold season and high in the warm season. The maximums occurred in June or September 2015, and August 2016, whilst the minimums occurred in December 2015, and February 2016 (Fig. 6a). In the warm season, RH had a weak positive linear relationship with elevation ($R^2 = 0.57$), and the rate of increase with elevation was $0.32\% \cdot 100\,m^{-1}$. The RH showed the opposite elevational gradient in the cold season, and the rate of decrease was $0.38\% \cdot 100\,m^{-1}$ ($R^2 = 0.81$). On a yearly scale, the correlation between RH and elevation had no obvious linear elevational gradient in the research catchment ($R^2 = 0.02$) (Fig. 6b).

3.1.5. Wind speed

The mean WS at the SN2980, SN3232, SN3711, SN4164 and SN4484 sites in 2015 and 2016 were $1.87\,m{\cdot}s^{-1}$, $2.18\,m{\cdot}s^{-1}$, $2.39\,m{\cdot}s^{-1}$, $2.82\,m{\cdot}s^{-1}$, and $2.92\,m{\cdot}s^{-1}$, respectively. Unlike RN, G, T and RH, the WS showed no apparent seasonal variation at the five research sites. WS in the cold season were slightly higher than those in the warm season at the SN2980, SN3232, SN3711 and SN4484, but not at the SN4164 site (Fig. 7a). The reason for this difference might be the presence of higher surrounding terrain around the SN4164 site, which might have caused a unique wind field and local circulation. The WS elevational gradients in the warm season, in the cold season and during the whole research period were $0.056\,m{\cdot}s^{-1}{\cdot}100\,m^{-1}$ ($R^2 = 0.90$), $0.083\,m{\cdot}s^{-1}{\cdot}100\,m^{-1}$ ($R^2 = 0.86$) and $0.069\,m{\cdot}s^{-1}{\cdot}100\,m^{-1}$ ($R^2 = 0.98$), respectively (Fig. 7b).

3.2. Elevational gradient of PET

According to the measured meteorological data from the five stations, the mean monthly PET values at the SN2980, SN3232, SN3711, SN4164 and SN4484 sites in 2015 and 2016 were $74.90\,mm{\cdot}month^{-1}$, $68.88\,mm{\cdot}month^{-1}$, $53.67\,mm{\cdot}month^{-1}$, $52.72\,mm{\cdot}month^{-1}$ and $47.27\,mm{\cdot}month^{-1}$, respectively. A slight difference was seen between 2015 and 2016; the total PET values at the five sites were 875.22 mm, 810.19 mm, 620.59 mm, 625.59 mm and 539.42 mm, respectively, in 2015, and 922.39 mm, 842.97 mm, 667.57 mm, 639.58 mm and 595.16 mm, respectively, in 2016.

Significant seasonal variation in PET (i.e., low in the cold season and high in the warm season) was seen at all five research sites. At the beginning of the year, the PET value was small, and it then increased until it reached the maximum in July before decreasing in the autumn and reach its minimum in December or January (Fig. 8).

The relationship between PET and elevation showed that PET decreased as elevation increased (Fig. 9). Analysis of the measured meteorological data showed that the topographic shading in mountainous region would influence the meteorological factors, especially the RN. In this study, the influences of topographic shading could not be ignored at the SN3711 and SN4164 sites in the cold season. Under these circumstances, all five sites were chosen for calculation of the PET elevational gradient for the warm season (Fig. 9a), and only three sites (SN2980, SN3232 and SN4484) were chosen for the calculation for the cold season and for the whole period (Fig. 9b). Thus, the PET elevational gradients for the warm season, the cold season and the whole
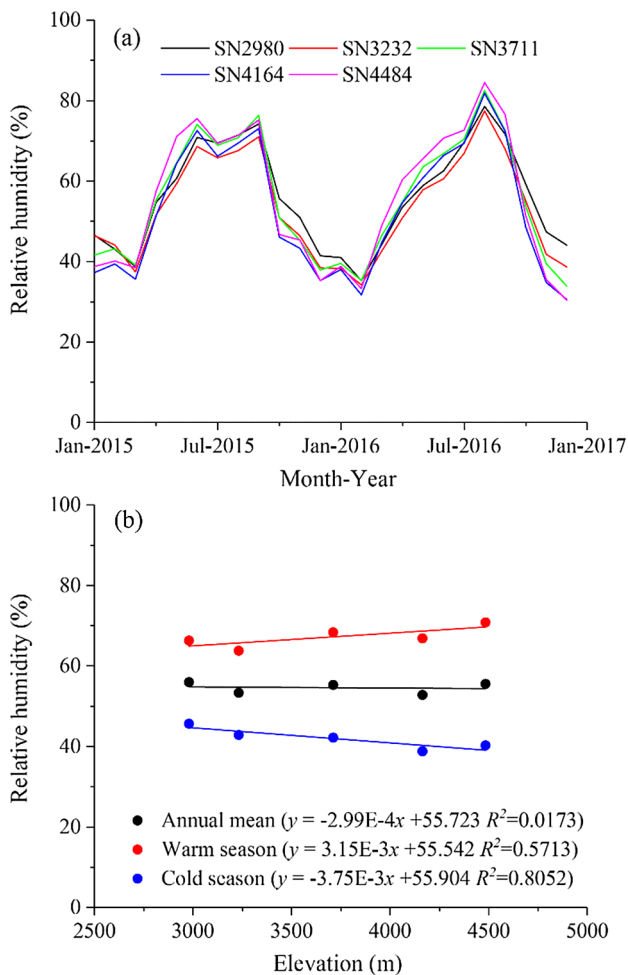
Fig. 6. Variations of in the monthly relative humidity (a) and the relationship between relative humidity and elevation (b) in the Hulu catchment.

period, were $-2.61\,\text{mm·month}^{-1}\cdot100\,\text{m}^{-1}$ ($R^2 > 0.98$), $-0.88\,\text{mm·month}^{-1}\cdot100\,\text{m}^{-1}$ ($R^2 > 0.99$) and $-1.80\,\text{mm·month}^{-1}\cdot100\,\text{m}^{-1}$ ($R^2 > 0.99$), respectively (Fig. 9).

3.3. Sensitivity analysis of PET to meteorological factors

3.3.1. SN2980

The RN, G, T, RH and WS values showed different sensitivities to the PET at the SN2980 site (Fig. 10a). Positive Srn and Su values for the whole research period indicated that the greater the RN and WS, the greater the PET. A negative of Srh value for the whole research period meant that the greater the RH, the smaller the PET. The Sg value was positive for most of the cold season and negative for most of the warm season. The G was usually positive in the warm season, and downward heat conduction towards relatively cold soil (conversely in the cold season). The greater the G value in the positive, the smaller the PET, and the greater the absolute value of G in the negative, the smaller the PET. The opposite phenomenon was shown by the St, which was positive for most of the warm season and negative for most of the cold season. When T was above 0 °C, the sensitivity of PET to T decreased as elevation increased. When T was below 0 °C, the sensitivity of PET to T increased as elevation increased. On a yearly scale, the St was negative at the SN2980 site.

The mean of the absolute values for Srn, Sg, St, Srh and Su showed that PET at the SN2980 site was most sensitive to RN, followed by RH, T, WS, and G during the whole period and in the warm season. The most sensitive meteorological factors in the cold season were RH and RN, followed by T, WS and G (Table 2).
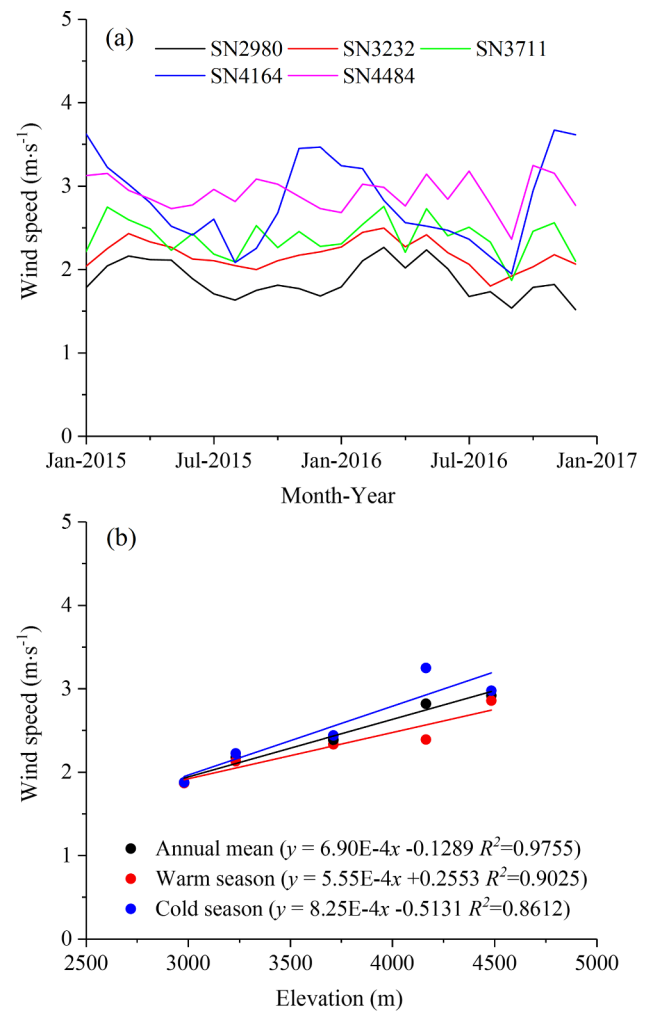

Fig. 7. Variations in the monthly wind speed (a) and the relationship between wind speed and elevation (b) in the Hulu catchment.

3.3.2. SN3232

Like the SN2980 site, the RN, G, T, RH and WS values showed different sensitivities to PET at the SN3232 site (Fig. 10b). The Sg, St, Srh and Su at the SN3232 site showed similar monthly variation to that of the SN2980 site, whilst the Srn showed a slight difference. In some cold months, such as January 2015, and December 2016, the RN was negative at the SN3232 site, and the Srn was also negative in those months. When RN was positive, the sensitivity of PET to RN decreased as elevation increased. When RN was negative, the sensitivity of PET to RN increased as elevation increased.

The mean values for Srn, Sg, St, Srh and Su showed that PET at the SN3232 site was most sensitive to RN, followed by RH, T, WS and G during the whole period and in the warm season. In the cold season, the most sensitive meteorological factors were T, followed by RH, WS, RN and G (Table 2).

3.3.3. SN3711

Like the SN2980 and SN3232 sites, the RN, G, T, RH and WS values showed different sensitivities to the PET at the SN3711 site (Fig. 10c). The Sg, St, Srh and Su values showed trends toward variation similar to that of the SN2980 site, whilst the Srn value was negative in some cold months because of the negative RN, as seen the SN3232 site. Because of topographic shading at the SN3711 site, the absolute value of the negative RN in the cold season was high and the PET was low. The absolute values for Srn, Sg, St, Srh and Su all showed significant increases in winter (Fig. 10c).
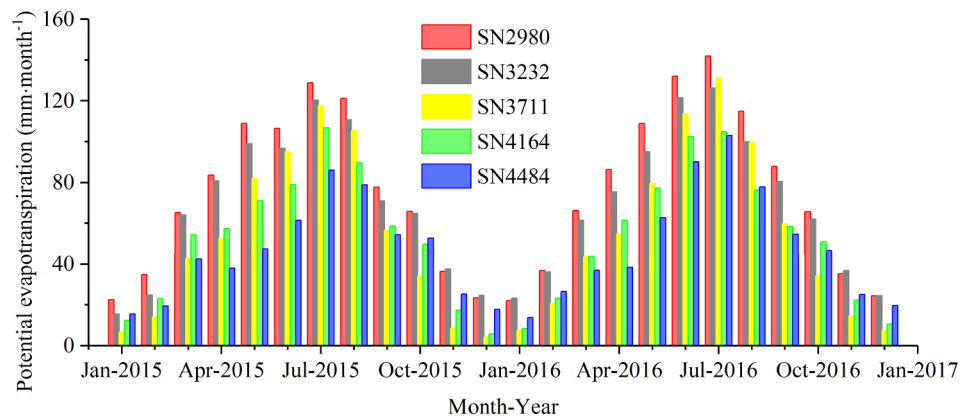
Fig. 8. Variations in the monthly potential evapotranspiration in the Hulu catchment.
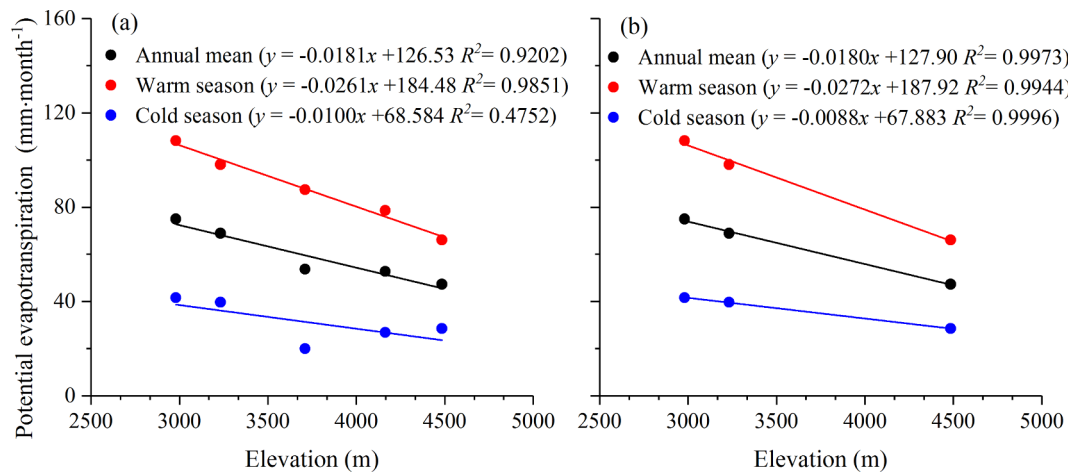

Fig. 9. Relationships between potential evapotranspiration and elevation at five (a) and three research sites (b) in the Hulu catchment.

The PET at the SN3711 site was most sensitive to RN, followed by RH, WS, T and G for the whole period and for the warm season. In the cold season, the most sensitive meteorological factor was RH, followed by RN, WS, T and G (Table 2).

3.3.4. SN4164

Like the SN3711 site, the RN, G, T, RH and WS values showed different sensitivities to the PET at the SN4164 site (Fig. 10d). Because of topographic shading, the absolute value of negative RN in the cold season was high, and the PET was low and the absolute values of Srn, Sg, St, Srh and Su all showed significant increases in winter at the SN4164 site (Fig. 10d).

The PET at the SN4164 site was most sensitive to RN, followed by RH, WS, T and G for the whole period and for the warm season. In the cold season, the most sensitive meteorological factor was RN, followed by WS, RH, T and G (Table 2).

3.3.5. SN4484

Because there was no obvious topographic shading, the variation trends of the Srn, Sg, St, Srh and Su values at the SN4484 site were more like the trends at the more-distant SN3232 site than those at nearer SN4164 site (Fig. 10e). Unlike the SN4164 site, the sensitivities of meteorological factors showed no obvious increase in winter. The Su values were positive and Srh values were negative throughout the whole research period. The Sg value was positive for most of the cold season and negative for most of the warm season. Conversely, the Srn and St values were negative for most of the cold season and positive for most of the warm season (Fig. 10e).

The PET at the SN4484 site was most sensitive to RH, followed by

RN, T, WS and G for the whole period. The sensitivity of meteorological factors at the SN4484 site in order of stronger to weaker was RN, RH, WS, T and G in the warm season, and T, RH, WS, RN and G in the cold season (Table 2).
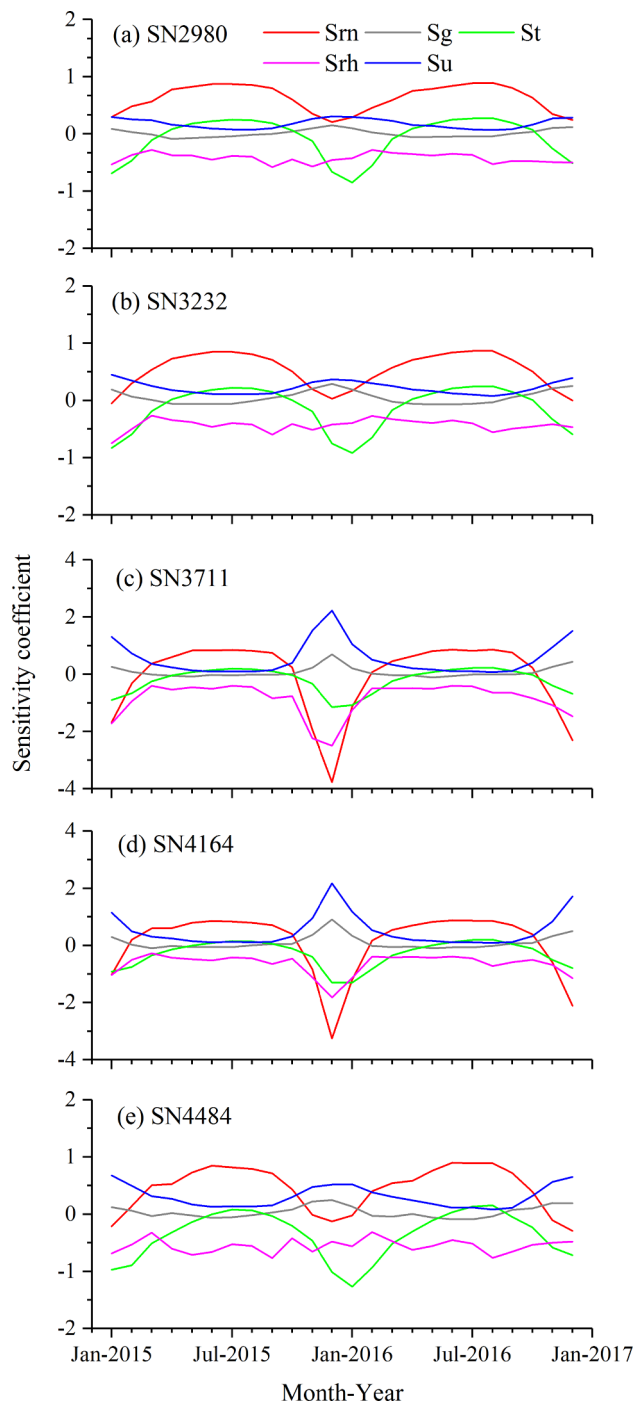
3.3.6. Catchment

As seen from the results from the five research sites for the whole yearly scale, the PET in the research region was most sensitive to RN, followed by RH, WS, T and G. The sensitivity of these characteristics in the research region, in order of stronger to weaker, was RN, RH, T, WS and G in the warm season, and RH, RN, WS, T and G in the cold season (Table 2). If the sites with topographic shading were removed and only SN2980, SN3232 and SN4484 were considered, the order of sensitivity would have been RN, RH, T, WS and G for the whole year and the warm season and T, RH, WS, RN and G for the cold season. If only the SN3711 and SN4164 sites were considered, the order of sensitivity in the regions with topographic shading was RN, RH, WS, T and G for the whole period, the warm season and the cold season. In all cases, the sensitivity of PET to G was weakest.

3.4. Elevational gradients of sensitivities of PET to meteorological factors

3.4.1. Net radiation

Because of topographic shading in the cold season at the SN3711 and SN4164 sites, all five sites were chosen to calculate the elevational gradient of Srn for the warm season (Fig. 11a), but only three sites were chosen for the cold season and for the whole period (Fig. 11b). Thus, the elevational gradients of Srn for the warm season, the cold season and the whole period were $-0.0033\cdot100\,\mathrm{m}^{-1}$ ($R^2 = 0.77$), $-0.016\cdot100\,\mathrm{m}^{-1}$ ($R^2 = 0.87$) and

Fig. 10. Variations in the monthly sensitivity coefficients of net radiation (Srn), soil heat flux (Sg), air temperature (St), relative humidity (Srh) and wind speed (Su) to potential evapotranspiration at the five research sites in the Hulu catchment.

$-0.010 \cdot 100\,\mathrm{m}^{-1}$ ($R^2 = 0.86$), respectively (Fig. 11). The negative Srn elevational gradient showed that the higher the elevation, the weaker the sensitivity of PET to RN. The RN was negative for a few months, and in this case, the higher the elevation, the greater the sensitivity of PET to RN.

3.4.2. Soil heat flux

Just as no significant linear elevational gradient of G was found in the research region for the cold season and for the whole period, the relationships between the Sg and elevation at five or three research sites showed there were no significant elevational gradient for the sensitivity

of PET to G (all $R^2 < 0.30$, Fig. 12). In the warm season, the elevational gradient of the Sg was $0.001 \cdot 100\,\mathrm{m}^{-1}$ in research region (Fig. 12a). The elevational gradient of the Sg was positive in the warm season, but Sg was negative for most of the warm season. Therefore, the higher the elevation, the weaker the sensitivity of PET to G in the warm season.

3.4.3. Air temperature

At all five or three research sites, the relationships between the St and elevation showed significant linear elevational gradients for the sensitivity of PET to T for the warm season, the cold season and the whole period (all $R^2 > 0.90$, Fig. 13). In the warm season, the elevational gradient of the St was $-0.015 \cdot 100\,\mathrm{m}^{-1}$ ($R^2 = 0.95$, Fig. 13a), and the negative elevational gradient meant that the higher the elevation, the weaker the sensitivity of PET to T. In the cold season and for the whole period, the elevational gradient of St was $-0.022 \cdot 100\,\mathrm{m}^{-1}$ and $-0.019 \cdot 100\,\mathrm{m}^{-1}$, respectively ($R^2 > 0.99$, Fig. 13b). The negative St value and its elevational gradient in the cold season and for the whole period meant that, if the T was below 0 °C, the higher the elevation, the greater sensitivity of PET to T.

3.4.4. Relative humidity

All Srh values were negative throughout the whole research period at all five research sites. Fig. 14 showed the relationships between the Srh values and elevation. As with Srn, all five sites were chosen to calculate the elevational gradient of Srh for the warm season (Fig. 14a), and only three sites were chosen for the cold season and for the whole period (Fig. 14b). The elevational gradients of Srh for the warm season, the cold season and the whole period were $-0.012 \cdot 100\,\mathrm{m}^{-1}$ ($R^2 = 0.82$), $-0.005 \cdot 100\,\mathrm{m}^{-1}$ ($R^2 = 0.99$) and $-0.009 \cdot 100\,\mathrm{m}^{-1}$ ($R^2 = 0.99$), respectively (Fig. 14). The negative Srh value and the negative Srh elevational gradient showed that the higher the elevation, the greater the sensitivity of PET to RH.

3.4.5. Wind speed

Fig. 15 showed the relationships between the Su value and elevation. The elevational gradients of Su for the warm season, the cold season and the whole research period were $0.003/100\,\mathrm{m}$ ($R^2 = 0.83$), $0.013/100\,\mathrm{m}$ ($R^2 = 0.99$) and $0.008/100\,\mathrm{m}$ ($R^2 = 0.98$), respectively (Fig. 15). The positive Su value and the positive Su elevational gradient meant that the higher the elevation, the greater the sensitivity of PET to WS.

4. Discussion

4.1. Sensitivity of PET to meteorological factors

The sensitivity of PET to meteorological factors is known to vary spatially among climate zones. The sensitivity of PET to the same factors showed significant variation from one climate location to another in the United States, including semiarid, Mediterranean-type, coastal humid, inland humid, semi-humid and island climates (Irmak et al., 2006). T was found to be the most important factor for PET in Australia, but the second-most important factors differed between dry and humid catchments (Guo et al., 2017). The most sensitive factor in China was RH, and great regional differences were seen (Liu et al., 2012). For example, the maximum temperature was the most sensitive factor in the Yellow River basin, Yangtze River basin and some other river basins, but RH was the most sensitive factor in the northwest river drainage system where this study area was located (Liu et al., 2012). The sensitivity of PET to meteorological factors is regional variation because climate conditions and meteorological factors from the different climate zones differ with regional variation. (Tabari and Talaee, 2014; Guo et al., 2017). This study showed that even in a small catchment, the sensitivity varied from low elevations to high elevations. On a yearly scale, RH and RN were the two most sensitive factors in catchment, but RH was more sensitive at high elevation and RN was more sensitive at

Table 2
Mean of absolute value of sensitivity of potential evapotranspiration to net radiation (Srn), soil heat flux (Sg), air temperature (St), relative humidity (Srh) and wind speed (Su) for the whole period, the warm season and the cold season at the five research sites.

Station	Annual mean					Warm season					Cold season				
	Srn	Sg	St	Srh	Su	Srn	Sg	St	Srh	Su	Srn	Sg	St	Srh	Su
SN2980	0.63	0.06	0.29	0.42	0.18	0.83	0.04	0.20	0.42	0.11	0.42	0.07	0.37	0.43	0.25
SN3232	0.54	0.10	0.30	0.43	0.22	0.79	0.05	0.16	0.43	0.13	0.29	0.14	0.44	0.43	0.31
SN3711	0.95	0.11	0.33	0.85	0.54	0.79	0.03	0.13	0.52	0.14	1.12	0.19	0.53	1.18	0.95
SN4164	0.86	0.15	0.37	0.64	0.50	0.79	0.05	0.11	0.50	0.14	0.94	0.26	0.64	0.79	0.86
SN4484	0.52	0.08	0.40	0.55	0.31	0.77	0.05	0.12	0.61	0.15	0.27	0.12	0.69	0.50	0.46
Mean	0.70	0.10	0.34	0.58	0.35	0.79	0.05	0.14	0.50	0.13	0.61	0.16	0.53	0.67	0.57

low elevation. Elevation strongly influences meteorological factors in high mountainous regions, thereby affecting PET and its sensitivity to meteorological factors.

The influences of elevation on the sensitivity of PET to meteorological factors have seldom been discussed. The sensitivity coefficients of maximum temperature and wind speed decreased as the elevation increased in Yellow River basin in China (Liu et al., 2012). In Wei River, a tributary of the Yellow River, RH and T were both more sensitive in the middle-lower region with a low elevation than upstream of the basin with a high elevation, and the sensitivities of solar radiation and WS showed seasonal variations (Zuo et al., 2012). In upper Mekong River basin, RH, T and WS were more sensitive in the middle-lower reaches, whilst the sensitivity of PET to the sunshine duration hours showed seasonal variation among the upper, middle and lower reaches (Li et al., 2015). The results of this study differed from those of other reports. For example, in this study, the sensitivities of PET to RH (Fig. 14) and WS (Fig. 15) both increased as the elevation increased, possibly because the earlier studies were based on data from national meteorological stations located in various climate regions; for example, the study of Yellow River used data from 77 meteorological stations in the basin with a length of 5464 km and a drainage area of 752443 km^2 (Liu et al., 2012). The research area in this study was a small catchment with area of 23.1 km^2, and the results were taken from five in situ meteorological stations at various elevations. The influence of elevation on PET sensitivity may differ with regional scale.

### 4.2. Influence of topographic shading on radiation in mountainous region

As a dominant energy source, solar radiation exerts a significant influence on the planet's energy and water cycles (Wang et al., 2018). In mountainous regions, the amount of solar radiation varies strongly with complex terrain (Chow et al., 2013) and controls water and heat

processes such as ET (Essery, 2004). To reduce the influence of topography on measurements of radiation and other meteorological factors, the meteorological stations must be built in open and flat part of mountainous areas as much as possible. However, topographic shading is widespread in mountainous regions. In this study, the solar elevation angles were high in the warm season, and no topographic shading was seen at any of the five meteorological stations. In the cold season, however, the solar elevation angles decreased, and the radiation sensors were usually shadowed by surrounding terrain while the sun rose at SN3711 and SN4164 sites (Fig. 16a). The time duration during which direct-beam solar radiation fell upon the SN3711 and SN4164 sites were the same as at the other three sites in the warm season, but were significantly shorter in the cold season (Fig. 16).

In addition to shortwave radiation, longwave radiation, including upward and downward radiation, is another key component to determine RN. The downward longwave radiation depends on the various gaseous layers in the atmosphere which are heated to a range of temperatures, and is controlled by air temperature and effective atmosphere emissivity. The upward longwave radiation depends on the emittance/absorptance properties of the material at the ground surface and its temperature (Ebrahimi and Marshall, 2015; Pashiardis et al., 2017). Because air temperature has a significant elevational gradient, and the ground surface temperature has a good correlation with air temperature (Yang et al., 2017b), the upward and downward longwave radiation at lower elevation sites (SN2980 and SN 3232) were significantly higher than those radiation at higher elevation sites (SN3711, SN4164 and SN 4484) (Fig. 17a and b). However, the upward and downward longwave radiation at higher elevation sites both showed weak difference, probably because there were many influencing factors to atmosphere emissivity and ground surface emissivity. Atmosphere emissivity is controlled by water vapor, carbon dioxide, ozone, cloud and dust (Allen et al., 1998; Masiri et al., 2017), and ground surface emissivity varies significantly as a result of differences in soil texture, mineral
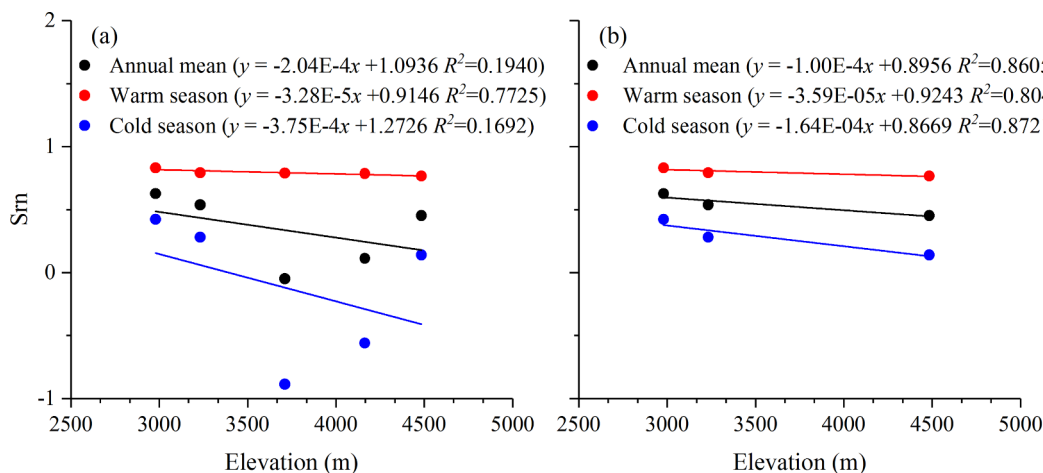
Fig. 11. Relationships between the sensitivity of potential evapotranspiration to the net radiation (Srn) and elevation at five (a) and three research sites (b) in the Hulu catchment.
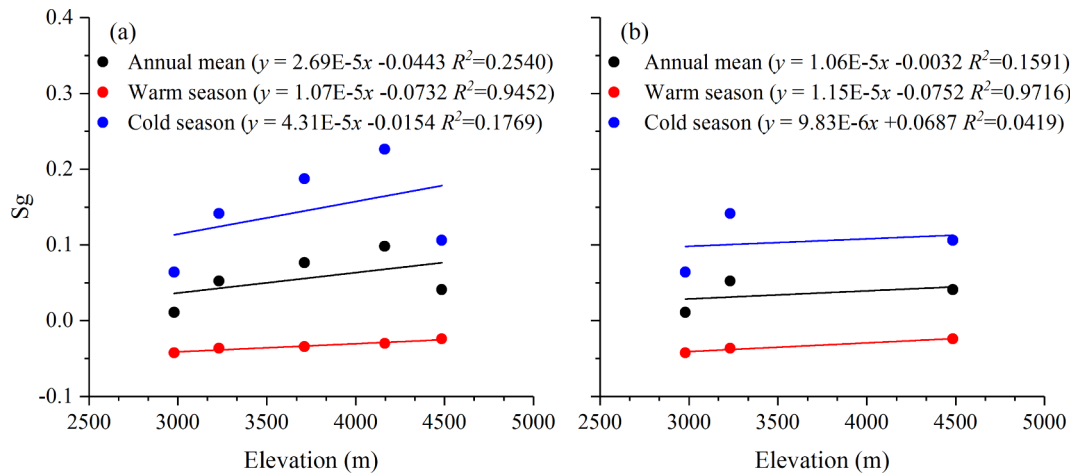
Fig. 12. Relationship between the sensitivity of potential evapotranspiration to the soil heat flux (Sg) and elevation at five (a) and three research sites (b) in the Hulu catchment.

composition organic and moisture content, and differences in plant cover (Van de Griend et al., 1991). The net longwave radiation, the difference between the upward and the downward longwave radiation, showed no obvious elevational gradient in the research region (Fig. 17c). Unlike the solar radiation, the net longwave radiations were not noticeably influenced by topographic shading. The RN at SN3711 and SN4164 sites in the cold season were not only significantly lower than that of SN2980 and SN3232 sites with lower elevation, but also lower than that of SN4484 site with higher elevation. The main reason for the relatively small RN in cold season at SN3711 and SN4164 sites was that the solar radiation was shielded by topographic shading. The obviously lower RN values at SN3711 and SN4164 sites because of topographic shading in the cold season influenced ET and its sensitivity to meteorological factors.

Terrain complexity is an important characteristic of mountains, and solar radiation was affected not only by cast shadowing in this study, but also by the slope and aspect of the terrain, atmospheric transmittance, albedo, sky view factor, and self-shadowing (Oliphant et al., 2003; Marsh et al., 2012). The influence of terrain on radiation in mountainous areas is extremely complex at the fine scale, and thus

forms a complex process of PET and its sensitivity to meteorological factors. Due to the lack of measurement data for meteorological factors under various topographic conditions, the results of this study focused only on the influences of elevation on PET and its sensitivity to meteorological factors.

5. Conclusions

In this study, the elevational gradients of meteorological factors such as net radiation (RN), soil heat flux (G), air temperature (T), relative humidity (RH), and wind speed (WS) were investigated based on measurement data from 2015 to 2016, from five automatic meteorological stations at various elevations in the Hulu catchment, Qilian Mountains. The RN and T decreased as the elevation increased in both warm and cold season, and WS increased as the elevation increased. Topographic shading by surrounding terrain significantly altered the direct solar radiation received at the surface, and reduced RN in the high mountainous regions. The RH in warm season increased as the elevation increased and but decreased in cold season. The G in warm
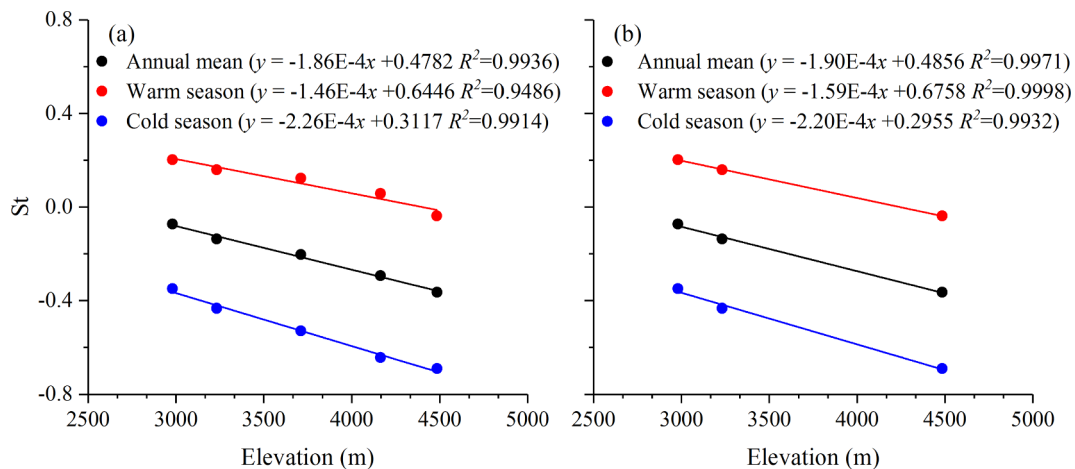
Fig. 13. Relationship between the sensitivity of potential evapotranspiration to air temperature (St) and elevation at five (a) and three research sites (b) in the Hulu catchment.
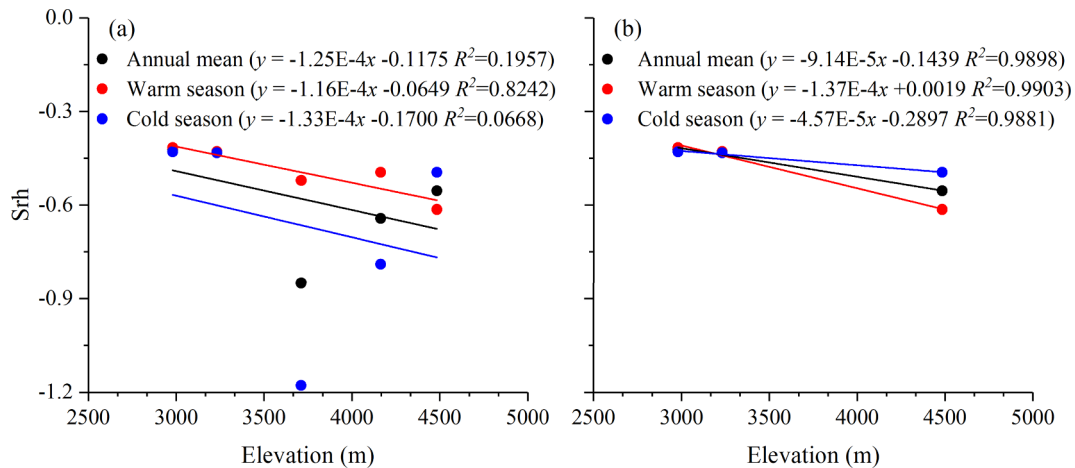
Fig. 14. Relationship between the sensitivity of potential evapotranspiration to relative humidity (Srh) and elevation at five (a) and three research sites (b) in the Hulu catchment.

season decreased as the elevation increased, whilst no significant elevational gradient were found for the cold season.

Potential evapotranspiration (PET) showed significant seasonal variation at all five research sites; it was low in the cold season and high in the warm season. The mean monthly PET values at the SN2980, SN3232, SN3711, SN4164 and SN4484 sites in 2015 and 2016 were 74.90 mm·month^{-1}, 68.88 mm·month^{-1}, 53.67 mm·month^{-1}, 52.72 mm·month^{-1} and 47.27 mm·month^{-1}, respectively. PET showed a significant elevational gradient, and decreased as the elevation increased. The sensitivity of meteorological factors to PET in the research region, in order of stronger to weaker, was RN, RH, T, WS and G for the whole period and the warm season and T, RH, WS, RN and G for the cold season. The sensitivity of G was significantly lower than that of the other meteorological factors.

The sensitivities of PET to meteorological factors showed different elevational gradients both in magnitude and direction. When the RN was positive, the sensitivity of PET to RN decreased as the elevation increased, and when the RN was negative, the sensitivity increased as

the elevation increased. When T was above 0 °C, the sensitivity of PET to T decreased as the elevation increased, and when T was below 0 °C, the sensitivity increased as the elevation increased. The higher the elevation, the greater the sensitivity of PET to both RH and WS. In warm season, the sensitivity of PET to G increased as the elevation increased, and the sensitivity did not show significant relationship with elevation in cold season. The RN was relatively small at the sites with topographic shading, and resulting in less sensitivity of PET to RN and greater sensitivity of PET to other meteorological factors.

The complex terrain in mountainous regions affects the water and heat transfer processes in the area, including ET. This study presents the effects of elevation on PET and its sensitivities to five meteorological factors. Future studies should consider the influences of other topographic factors on PET, such as slope and aspect, to contribute to our understanding of the influences of complex terrain on ET and water cycle and to provide some scientific basis for water source and environmental protection in mountainous regions.
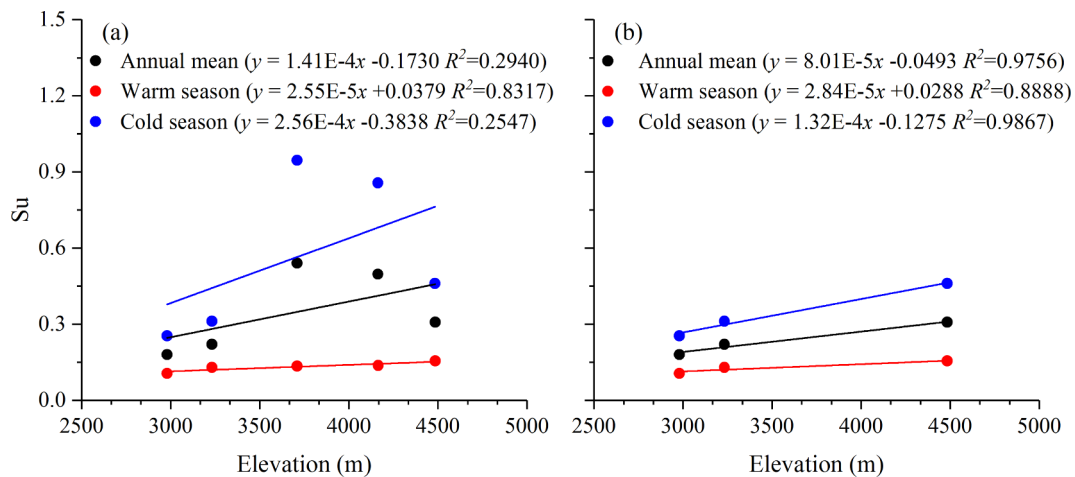
Fig. 15. Relationship between the sensitivity of potential evapotranspiration to wind speed (Su) and elevation at five (a) and three research sites (b) in the Hulu catchment.
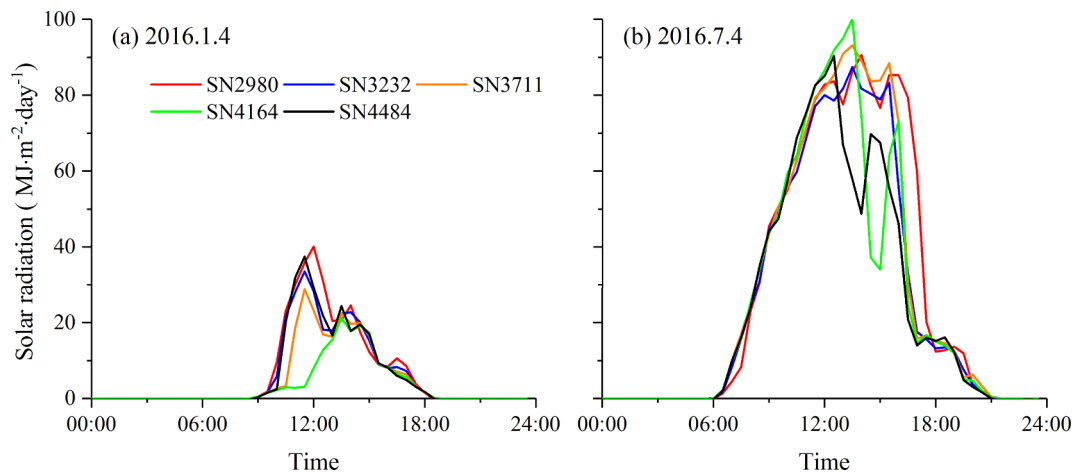
Fig. 16. Diurnal variations in solar radiation at five research sites on January 4, 2016 (a) and July 4, 2016 (b).
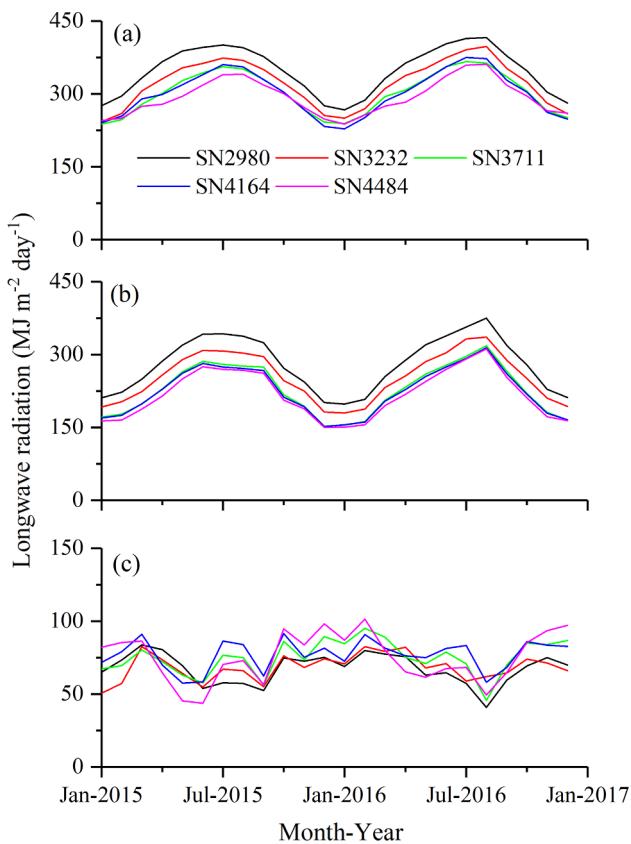

Fig. 17. Variations in the monthly upward longwave radiation (a), downward longwave radiation (b) and net longwave radiation (c) at five research sites in the Hulu catchment.

Acknowledgments

Appendix A. Supplementary data

Supplementary data to this article can be found online at https://doi.org/10.1016/j.jhydrol.2018.10.069.

References

Allen, R.G., 2006. Evaporation modeling: potential. In: Anderson, M.G. (Ed.), Encyclopedia of Hydrological Sciences. Wiley, Chichester, UK.

Allen, R.G., Pereira, L.S., Raes, D., Smith, M., 1998. Crop evapotranspiration–Guidelines for computing crop water requirements. FAO Irrigation and Drainage Paper 56, Rome, Italy.

Almorox, J., Quej, V.H., Martí, P., 2015. Global performance ranking of temperature-based approaches for evapotranspiration estimation considering Köppen climate classes. J. Hydrol. 528, 514–522. https://doi.org/10.1016/j.jhydrol.2015.06.057.

Beniston, M., Stoffel, M., 2014. Assessing the impacts of climatic change on mountain water resources. Sci. Total Environ. 493, 1129–1137. https://doi.org/10.1016/j.scitotenv.2013.11.122.

Burn, D.H., Hesch, N.M., 2007. Trends in evaporation for the Canadian Prairies. J. Hydrol. 336 (1–2), 61–73. https://doi.org/10.1016/j.jhydrol.2006.12.011.

Chen, R.S., Song, Y.X., Kang, E.S., Han, C.T., Liu, J.F., Yang, Y., Qing, W.W., Liu, Z.W., 2014. A cryosphere-hydrology observation system in a small alpine watershed in the Qilian Mountains of China and its meteorological gradient. Arct. Antarct. Alp. Res. 46 (2), 505–523. https://doi.org/10.1657/1938-4246-46.2.505.

Chow, F.K., DeWekker, S.F.J., Snyder, B.J., 2013. Mountain Weather Research and Forecasting. Springer, Dordrecht.

Dettinger, M., 2014. Climate change: Impacts in the third dimension. Nat. Geosci. 7 (3), 166–167. https://doi.org/10.1038/ngeo2096.

Dodson, R., Marks, D., 1997. Daily air temperature interpolated at high spatial resolution over a large mountainous region. Clim. Res. 8, 1–20. https://doi.org/10.3354/cr008001.

Dong, L., Zhang, M., Wang, S., Qiang, F., Zhu, X., Ren, Z., 2015. The freezing level height in the Qilian Mountains, northeast Tibetan Plateau based on reanalysis data and observations, 1979–2012. Quat. Int. 380–381, 60–67. https://doi.org/10.1016/j.quaint.2014.08.049.

Donohue, R.J., McVicar, T.R., Roderick, M.L., 2010. Assessing the ability of potential evaporation formulations to capture the dynamics in evaporative demand within a changing climate. J. Hydrol. 386 (1–4), 186–197. https://doi.org/10.1016/j.jhydrol.2010.03.020.

Douglas, E.M., Jacobs, J.M., Sumner, D.M., Ray, R.L., 2009. A comparison of models for estimating potential evapotranspiration for Florida land cover types. J. Hydrol. 373 (3–4), 366–376. https://doi.org/10.1016/j.jhydrol.2009.04.029.

Ebrahimi, S., Marshall, S.J., 2015. Parameterization of incoming longwave radiation at glacier sites in the Canadian Rocky Mountains. J. Geophys. Res. [Atmos.] 120, 136–12556. https://doi.org/10.1002/2015JD023324.

Essery, R., 2004. Statistical representation of mountain shading. Hydrol. Earth Syst. Sci. 8 (6), 1045–1050.

Feng, Q., 2010. Water Resources in the Hexi Corridor and Its Cycle. In: Sumi, A., Fukushi, K., Honda, R., Hassan, K.M. (Eds.), Sustainability in Food and Water: An Asian Perspective. Springer, Netherlands, Dordrecht, pp. 299–310.

Guo, D., Westra, S., Maier, H.R., 2017. Sensitivity of potential evapotranspiration to changes in climate variables for different Australian climatic zones. Hydrol. Earth Syst. Sci. 21 (4), 2107–2126. https://doi.org/10.5194/hess-21-2107-2017.

Irmak, S., Payero, J.O., Martin, D.L., Irmak, A., Howell, T.A., 2006. Sensitivity analyses and sensitivity coefficients of standardized daily ASCE-Penman-Monteith equation. J Irrig. Drain. E-ASCE 132 (6), 264–578. https://doi.org/10.1061//asce/0733-9437/

2006/132:6/564.

Lhomme, J.P., 1997. Towards a rational definition of potential evaporation. Hydrol. Earth Syst. Sci. 1 (2), 257–264.

Li, B., Chen, F., Guo, H., 2015. Regional complexity in trends of potential evapo-transpiration and its driving factors in the Upper Mekong River Basin. Quat. Int. 380–381, 83–94. https://doi.org/10.1016/j.quaint.2014.12.052.

Li, S., Kang, S., Zhang, L., Zhang, J., Du, T., Tong, L., Ding, R., 2016. Evaluation of six potential evapotranspiration models for estimating crop potential and actual eva-potranspiration in arid regions. J. Hydrol. 543, 450–461. https://doi.org/10.1016/j.jhydrol.2016.10.022.

Li, X., Wang, L., Chen, D., Yang, K., Wang, A., 2014. Seasonal evapotranspira-ion changes (1983–2006) of four large basins on the Tibetan Plateau. J. Geophys. Res. [Atmos.] 119, 13079–13095. https://doi.org/10.1002/.

Li, C., Wu, P.T., Li, X.L., Zhou, T.W., Sun, S.K., Wang, Y.B., Luan, X.B., Yu, X., 2017. Spatial and temporal evolution of climatic factors and its impacts on potential eva-potranspiration in Loess Plateau of Northern Shaanxi. China. Sci. Total Environ. 589, 165–172. https://doi.org/10.1016/j.scitotenv.2017.02.122.

Liu, C., Zhang, D., Liu, X., Zhao, C., 2012. Spatial and temporal change in the potential evapotranspiration sensitivity to meteorological factors in China (1960–2007). J. Geogr. Sci. 22 (1), 3–14. https://doi.org/10.1007/s11442-012-0907-4.

Marsh, C.B., Pomeroy, J.W., Spiteri, R.J., 2012. Implications of mountain shading on calculating energy for snowmelt using unstructured triangular meshes. Hydrol. Process. 26 (12), 1767–1778. https://doi.org/10.1002/hyp.9329.

Masiri, I., Janjai, S., Nunez, M., Anusasananan, P., 2017. A technique for mapping downward longwave radiation using satellite and ground-based data in the tropics. Renew. Energy 103, 171–179. https://doi.org/10.1016/j.renene.2016.11.018.

McCuen, R.H., 1974. A sensitivity and error analysis of procedures used for estimating evaporation. Water Resour. Bull. 10 (3), 486–498.

McVicar, T.R., Roderick, M.L., Donohue, R.J., Li, L.T., Van Niel, T.G., Thomas, A., Grieser, J., Jhajharia, D., Himri, Y., Mahowald, N.M., Mescherskaya, A.V., Kruger, A.C., Rehman, S., Dinpashoh, Y., 2012. Global review and synthesis of trends in observed terrestrial near-surface wind speeds: implications for evaporation. J. Hydrol. 416–417, 182–205. https://doi.org/10.1016/j.jhydrol.2011.10.024.

Milano, M., Reynard, E., Koplin, N., Weingartner, R., 2015. Climatic and anthropogenic changes in Western Switzerland: Impacts on water stress. Sci. Total Environ. 536, 12–24. https://doi.org/10.1016/j.scitotenv.2015.07.049.

Milly, P.C.D., Dunne, K.A., 2016. Potential evapotranspiration and continental drying. Nat. Clim. Change 6 (10), 946–949. https://doi.org/10.1038/nclimate3046.

Mountain Research Initiative EDW Working Group, 2015. Elevation-dependent warming in mountain regions of the world. Nat. Clim. Change 5 (5), 424–430. https://doi.org/10.1038/nclimate2563.

Oliphant, A.J., Spronken-Smithb, R.A., Sturmanb, A.P., Owensb, I.F., 2003. Spatial variability of surface radiation fluxes in mountainous terrain. J. Appl. Meteorol. 42 (1), 113–128.

Paparrizos, S., Maris, F., Matzarakis, A., 2016. Sensitivity analysis and comparison of various potential evapotranspiration formulae for selected Greek areas with different climate conditions. Theor. Appl. Climatol. 128 (3–4), 745–759. https://doi.org/10.1007/s00704-015-1728-z.

Pashiardis, S., Kalogirou, S.A., Pelengaris, A., 2017. Characteristics of longwave radiation through the statistical analysis of downward and upward longwave radiation and inter-comparison of two sites in Cyprus. J. Atmos. Sol.-Terr. Phys. 164, 60–80. https://doi.org/10.1016/j.jastp.2017.08.007.

Peng, S., Ding, Y., Wen, Z., Chen, Y., Cao, Y., Ren, J., 2017. Spatiotemporal change and trend analysis of potential evapotranspiration over the Loess Plateau of China during 2011–2100. Agric. For. Meteorol. 233, 183–194. https://doi.org/10.1016/j.agrformet.2016.11.129.

Ragettlia, S., Immerzeelb, W.W., Pellicciotti, F., 2016. Contrasting climate change impact on river flows from high-altitude catchments in the Himalayan and Andes Mountains. P. Natl. Acad. Sci. U. S. A. 113 (33), 9222–9227.

Robinson, E.L., Blyth, E.M., Clark, D.B., Finch, J., Rudd, A.C., 2017. Trends in atmo-spheric evaporative demand in Great Britain using high-resolution meteorological data. Hydrol. Earth Syst. Sci. 21 (2), 1189–1224. https://doi.org/10.5194/hess-21-1189-2017.

Roderick, M.L., Rotstayn, L.D., Farquhar, G.D., Hobbins, M.T., 2007. On the attribution of changing pan evaporation. Geophys. Res. Lett. 34 (17). https://doi.org/10.1029/2007gl031166.

Rogora, M., Frate, L., Carranza, M.L., Freppaz, M., Stanisci, A., Bertani, I., Bottarin, R., Brambilla, A., Canullo, R., Carbognani, M., Cerrato, C., Chelli, S., Cremonese, E., Cutini, M., Di Musciano, M., Erschbamer, B., Godone, D., Iocchi, M., Isabellon, M., Magnani, A., Mazzola, L., Morra di Cella, U., Pauli, H., Petey, M., Petriccione, B., Porro, F., Psenner, R., Rossetti, G., Scotti, A., Sommaruga, R., Tappeiner, U., Theurillat, J.P., Tomaselli, M., Viglietti, D., Viterbi, R., Vittoz, P., Winkler, M., Matteucci, G., 2018. Assessment of climate change effects on mountain ecosystems through a cross-site analysis in the Alps and Apennines. Sci. Total Environ. 624, 1429–1442. https://doi.org/10.1016/j.scitotenv.2017.12.155.

Senay, G.B., Leake, S., Nagler, P.L., Artan, G., Dickinson, J., Cordova, J.T., Glenn, E.P., 2011. Estimating basin scale evapotranspiration (ET) by water balance and remote sensing methods. Hydrol. Process. 25 (26), 4037–4049. https://doi.org/10.1002/

hyp.8379.

Sun, S., Chen, H., Wang, G., Li, J., Mu, M., Yan, G., Xu, B., Huang, J., Wang, J., Zhang, F., Zhu, S., 2016. Shift in potential evapotranspiration and its implications for dryness/wetness over Southwest China. J. Geophys. Res. [Atmos.] 121 (16), 9342–9355. https://doi.org/10.1002/2016jd025276.

Tabari, H., Talaee, P.H., 2014. Sensitivity of evapotranspiration to climatic change in different climates. Global Planet. Change 115, 16–23. https://doi.org/10.1016/j.gloplacha.2014.01.006.

Tabari, H., Aeini, A., Talaee, P.H., Some'e, B.S., 2012. Spatial distribution and temporal variation of reference evapotranspiration in arid and semi-arid regions of Iran. Hydrol. Process. 26 (4), 500–512. https://doi.org/10.1002/hyp.8146.

Van de Griend, A.A., Owe, M., Groen, M., Stoll, M.P., 1991. Measurement and spatial variation of thermal infrared surface emissivity in a savanna environment. Water Resour. Res. 27 (3), 371–379. https://doi.org/10.1029/90WR02616.

van den Bergh, T., Inauen, N., Hiltbrunner, E., Körner, C., 2013. Climate and plant cover co-determine the elevational reduction in evapotranspiration in the Swiss Alps. J. Hydrol. 500, 75–83. https://doi.org/10.1016/j.jhydrol.2013.07.013.

Viviroli, D., Dürr, H.H., Messerli, B., Meybeck, M., Weingartner, R., 2007. Mountains of the world, water towers for humanity: Typology, mapping, and global significance. Water Resour. Res. 43 (7), W07447. https://doi.org/10.1029/2006wr005653.

Viviroli, D., Archer, D.R., Buytaert, W., Fowler, H.J., Greenwood, G.B., Hamlet, A.F., Huang, Y., Koboltschnig, G., Litaor, M.I., López-Moreno, J.I., Lorentz, S., Schädler, B., Schreier, H., Schwaiger, K., Vuille, M., Woods, R., 2011. Climate change and mountain water resources: overview and recommendations for research, manage-ment and policy. Hydrol. Earth Syst. Sci. 15 (2), 471–504. https://doi.org/10.5194/hess-15-471-2011.

Wang, Y., Jiang, T., Bothe, O., Fraedrich, K., 2007. Changes of pan evaporation and re-ference evapotranspiration in the Yangtze River basin. Theor. Appl. Climatol. 90 (1–2), 13–23. https://doi.org/10.1007/s00704-006-0276-y.

Wang, W., Xing, W., Shao, Q., Yu, Z., Peng, S., Yang, T., Yong, B., Taylor, J., Singh, V.P., 2013. Changes in reference evapotranspiration across the Tibetan Plateau: observa-tions and future projections based on statistical downscaling. J. Geophys. Res. [Atmos.] 118 (10), 4049–4068. https://doi.org/10.1002/jgrd.50393.

Wang, W., Li, C., Xing, W., Fu, J., 2017. Projecting the potential evapotranspiration by coupling different formulations and input data reliabilities: the possible uncertainty source for climate change impacts on hydrological regime. J. Hydrol. 555, 298–313. https://doi.org/10.1016/j.jhydrol.2017.10.023.

Wang, Q., Wang, J., Zhao, Y., Li, H., Zhai, J., Yu, Z., Zhang, S., 2016. Reference evapo-transpiration trends from 1980 to 2012 and their attribution to meteorological dri-vers in the three-river source region. China. Int. J. Climatol. 36 (11), 3759–3769. https://doi.org/10.1002/joc.4589.

Wang, T., Yan, G., Mu, X., Jiao, Z., Chen, L., Chu, Q., 2018. Toward operational short-wave radiation modeling and retrieval over rugged terrain. Remote Sens. Environ. 205, 419–433. https://doi.org/10.1016/j.rse.2017.11.006.

Woo, M., 2008. Cold region atmospheric and hydrologic studies. The Mackenzie GEWEX Experience, Volume 2: Hydrologic Processes. Springer Berlin Heidelberg, New York.

Xu, C.Y., Singh, V.P., 2002. Cross Comparison of Empirical Equations for Calculating Potential Evapotranspiration with Data from Switzerland. Water Resour. Manage. 16, 197–219.

Yang, Y., Chen, R., Song, Y., Liu, J., Han, C., Liu, Z., 2017b. New methods for calculating bare soil land surface temperature over mountainous terrain. J. Mt. Sci. 14 (12), 2471–2483. https://doi.org/10.1007/s11629-016-4306-7.

Yang, Y., Chen, R., Song, Y., Han, C., Liu, J., Liu, Z., 2017a. Actual daily evapo-transpiration and crop coefficients for an alpine meadow in the Qilian Mountains, northwest China. Hydrol. Res. 48 (4), 1131–1142. https://doi.org/10.2166/nh.2016.124.

Yin, Y., Wu, S., Dai, E., 2010. Determining factors in potential evapotranspiration changes over China in the period 1971–2008. Chinese Sci. Bull. 55 (29), 3329–3337. https://doi.org/10.1007/s11434-010-3289-y.

Yin, Y., Wu, S., Zhao, D., 2013. Past and future spatiotemporal changes in evapo-transpiration and effective moisture on the Tibetan Plateau. J. Geophys. Res. [Atmos.] 118 (19), 10850–10860. https://doi.org/10.1002/jgrd.50858.

Zhang, D., Liu, X., Hong, H., 2013. Assessing the effect of climate change on reference evapotranspiration in China. Stoch. Environ. Res. Risk Assess. 27 (8), 1871–1881. https://doi.org/10.1007/s00477-013-0723-0.

Zheng, H., Yu, G., Wang, Q., Zhu, X., Yan, J., Wang, H., Shi, P., Zhao, F., Li, Y., Zhao, L., Zhang, J., Wang, Y., 2017. Assessing the ability of potential evapotranspiration models in capturing dynamics of evaporative demand across various biomes and climatic regimes with ChinaFLUX measurements. J. Hydrol. 551, 70–80. https://doi.org/10.1016/j.jhydrol.2017.05.056.

Zhou, X., Li, X., John, D., Zhao, K., 2016. Rapid agricultural transformation in the pre-historic Hexi corridor. China. Quatern. Int. 426, 33–41. https://doi.org/10.1016/j.quaint.2016.04.021.

Zuo, D., Xu, Z., Yang, H., Liu, X., 2012. Spatiotemporal variations and abrupt changes of potential evapotranspiration and its sensitivity to key meteorological variables in the Wei River basin. China. Hydrol. Process. 26 (8), 1149–1160. https://doi.org/10.1002/hyp.8206.